

## Charge transfer model for quadrupole interactions and binding energies of point defects with $^{111}\text{In}/\text{Cd}$ probes in cubic metals

Gary S. Collins and Matthew O. Zacate

Department of Physics, Washington State University, Pullman, WA 99164-2814, USA

Email: collins@wsu.edu

A simple model is used to predict nuclear quadrupole interactions caused by point defects at near-neighbor sites of probe atoms in cubic, metallic hosts. Also predicted are binding energies between the defects and impurity probe atoms. The model assumes that electrostatic interactions predominate over strain interactions. It is critically examined using data for  $^{111}\text{In}/\text{Cd}$  probes next to solute atoms in noble metal hosts, obtained mostly by K. Królas, and next to vacancies in metals and intermetallic phases. The magnitude of quadrupole interactions is found to correlate well with charge transfer between host metal and defect. Charge transfer is taken to be proportional to the difference between work functions of the defect and host elements. An *ansatz* is proposed for the work function of a vacancy. Good correlations are obtained between experimental and calculated interactions for the generally oversized  $^{111}\text{In}/\text{Cd}$  probe. The charge transfer model is believed to be applicable for other probes that are oversized.

**Keywords:** *quadrupole interaction, electric field gradient, point defect*

*On the occasion of the 80<sup>th</sup> birthday of Hendrik de Waard*

### 1. Introduction

Nuclear hyperfine interaction methods have been applied over three decades to study point defects in metals and intermetallic compounds. The measurements yield information about electric field gradient (efg) tensors at probe nuclei that arise from the defects, which are generally described via the principal component  $V_{zz}$  (called the efg, for short) and efg asymmetry parameter  $\eta = |(V_{xx} - V_{yy})/V_{zz}|$ . When there is at least a three-fold axis of charge symmetry through the probe nucleus,  $\eta = 0$  and the fundamental precession frequency of the quadrupole moment  $Q$  of a nucleus of spin  $5/2$  measured using perturbed angular correlation of gamma rays (PAC) is given by  $\omega_0 = |\frac{3\pi}{10} eQV_{zz}|$ . (The sign of the efg cannot be measured using PAC). Quadrupole interaction parameters  $\omega_0$  and  $\eta$  serve as labels of different defect-probe bound states. The principal other measurable is the signal amplitude, which is directly proportional to the fraction of the probe nuclei in the corresponding local environment. In a simple measurement, for example, there may be site fractions  $f_0$  and  $f_1$  of probe atoms having 0 and 1 defect in the first neighbor shell. For impurity probes, the site fraction will be affected by the interaction between probe and defect that is characterized by a binding energy  $E_B$ . Generally, only defects in the first atomic shell produce large quadrupole and binding interactions.

Magnitudes of quadrupole interactions of related defect configurations, such as vacancies next to a specified probe in different *fcc* metals or different solutes next to a specified probe in a given host, have been found to vary greatly, and no simple method has been available to predict relative quadrupole interactions with an accuracy of the order of  $\pm 30\%$ . At a more sophisticated level, modern electronic band-structure programs such as Wien2k [1] make it possible in principle to calculate binding energies and electric field gradients for probe-defect complexes. However, such calculations are time consuming. In the present paper, we develop a simple method to predict such interactions.

Defect charge and size have been considered traditionally important empirical parameters that affect efgs. For metals, the charge associated with a defect is problematic. The Wigner-Seitz cell surrounding each site in a pure metal is, of course, neutral. In general, charge is transferred between the host metal and a defect or probe atom, leading to a non-zero defect charge and local electrostatic potential. Mismatch between the size of a defect and host atom may lead to isotropic and/or lower-symmetry atomic relaxations around the defect and also affect quadrupole or binding interactions. In the present paper, a simple electrostatic model is found to predict quadrupole and binding interactions without the need to include local atomic relaxations. The model is evaluated critically using data measured with the  $^{111}\text{In}/\text{Cd}$  PAC probe and found to work well. However, the model is unsuccessful explaining data obtained using the  $^{100}\text{Pd}/\text{Rh}$  probe. The difference is attributed to dissimilar local lattice relaxations around oversized ( $^{111}\text{In}/\text{Cd}$ ) and undersized ( $^{100}\text{Pd}/\text{Rh}$ ) probes.

## 2. Charge Transfer

A defect is assumed to take on a net charge that produces an electrostatic potential at nearby probe nuclei, which for simplicity is assumed to be coulombic. Given a defect charge  $Q_D$ , the quadrupole interaction is then in first approximation proportional to  $Q_D/\Omega_H$ , in which  $\Omega_H$  is the atomic volume of the host and accounts for both the  $r^{-3}$  dependence of the efg and the host lattice parameter. Given the charge of the impurity probe  $Q_P$ , the binding energy of a near-neighbor probe-defect pair is proportional to  $Q_P Q_D / \Omega_H^{1/3}$ . Lattice relaxation is ignored, in which case the expected efg asymmetry parameter is zero. Effects of lattice relaxation will be considered further below.

Defect charges are calculated using a charge transfer mechanism motivated by Miedema's semi-empirical enthalpy model [2]. That model was developed to calculate enthalpies of alloy formation and has been extended to calculate properties of solids such as surface and vacancy formation energies and Mössbauer isomer shifts [2]. A clear exposition of the Miedema model has been given in a recent monograph by Hans Bakker [3]. The basic concept of Miedema's model is to treat atoms as 'blocks' having macroscopic properties of the corresponding elements. Three fundamental parameters are posited: the work function  $\phi$ , density of states at the Wigner-Seitz boundary of the atomic cell, and molar volume. Interactions occur at interfaces of dissimilar atoms that reduce the energy of the system. These include charge transfer between atoms A and B that is conceptually driven in the Miedema model by the difference in work functions of the two elements,  $\phi_A - \phi_B$ , with electrons transferring from

atoms of the element having the smaller work function to atoms of the element having the greater work function, as illustrated in Fig. 1. An elaborate method for calculating charge transfer is part of the Miedema model, and includes a volume change associated with charge transfer and an additional volume change caused by elastic response of the impurity atom and host to accommodate a mismatch in atomic volume [2,3]. Here, we assume more simply that the charge of a defect is proportional to the difference in work functions of defect and host. This very simple parameterization was found to lead to greater consistency between model predictions and measurement than more elaborate calculations carried out using the Miedema model.

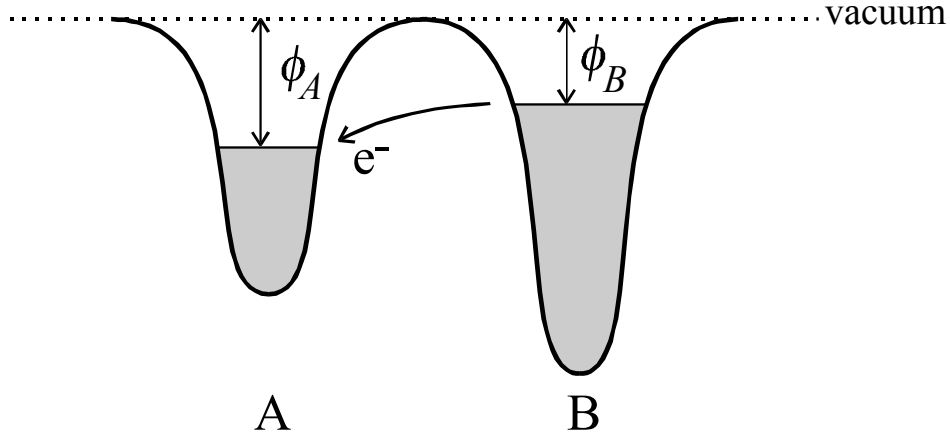


Figure 1. Schematic illustration of adjacent atoms A and B with work functions  $\phi_A$  and  $\phi_B$ . Energy is reduced by transfer of electrons to the atom having the greater work function (atom A as drawn). Atom A takes on a negative charge proportional to  $\phi_B - \phi_A$ .

The defect charge of a solute  $S$  in host  $H$  thus is assumed to be proportional to the difference of work functions  $\phi_H - \phi_S \equiv \Delta\phi_{HS}$ , with a positive value corresponding to a positive charge of the solute. Assuming a coulombic interaction, the electric field gradient,  $V_{zz}$ , at the nucleus of the probe atom  $P$ , is then given by

$$V_{zz} \propto \Delta\phi_{HS} / \Omega_H, \quad (1)$$

in which  $\Omega_H$  is the atomic volume of a host atom. The fundamental quadrupole interaction frequency  $\omega_0$  is given by

$$\omega_0 \propto |V_{zz}| \propto |\Delta\phi_{HS} / \Omega_H|. \quad (2)$$

Taking the probe charge to be proportional to  $\phi_H - \phi_P \equiv \Delta\phi_{HP}$  and assuming a coulombic interaction, one obtains for the binding energy  $E_B$  the proportionality

$$E_B \propto -\Delta\phi_{HP}\Delta\phi_{HS} / \Omega_H^{1/3}, \quad (3)$$

in which a negative sign has been inserted to establish the convention that positive values of  $E_B$  correspond to attractive interactions. Equations 2 and 3 are used below to estimate  $\omega_0$  and  $E_B$  for solutes.

A vacancy defect lacks an obvious definition for its work function. Conceptually, a vacancy arises by cutting an atom out of the solid, after which electrons flow in from the surrounding host, giving it a negative charge. It is reasonable to assume that the effective work function of a vacancy lies between the work function of the host and the work function of the host plus the host's Fermi energy  $E_F$ . As an *ansatz*, the work function of a vacancy is taken to be greater than the work function of the host by a fraction  $f$  of the host's Fermi energy  $E_F$  that is universal for all metals. This is illustrated schematically in Fig. 2, and leads to a difference between work functions of the host and vacancy equal to  $\phi_H - \phi_V \equiv \Delta\phi_{HV} = \phi_H - (\phi_H + f \cdot E_F) = -f \cdot E_F$ . Such a linear (or at least monotonic) dependence of  $\phi_H - \phi_V$  on  $E_F$  is expected because electrostatic screening of defects is more effective in metals with a greater bandwidth ( $E_F$ ). Note that  $\Delta\phi_{HV}$  is negative, indicating that electrons flow into the vacancy, giving it a negative charge. Expressions for  $\omega_0$  and  $E_B$  for vacancies are therefore the same as eqs. 2 and 3, but in which  $\Delta\phi_{HS}$  is replaced by  $\Delta\phi_{HV} = -f \cdot E_F$ .

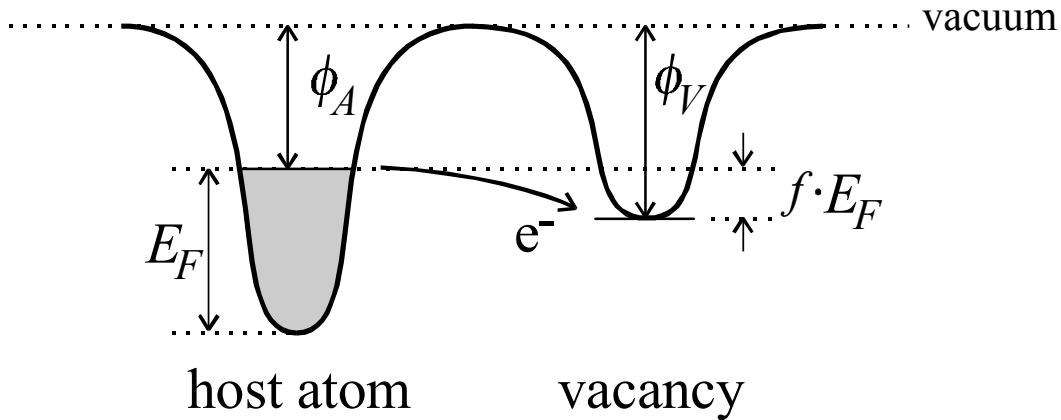


Figure 2. Charge transfer from metal atoms in host A to a vacancy. The amount of charge transferred to the vacancy is assumed to be proportional to the Fermi energy  $E_F$  of conduction electrons in host A.

As shown below, selecting  $f=0.20$  leads to a consistent description of quadrupole interactions measured for both solutes and vacancies using the  $^{111}\text{Cd}$  probe.

The charge transfer model was implemented for solutes using a standardized set of work functions developed for the Miedema model [2,3]. Table I lists Miedema work functions, an optimized set of work functions described below, and Wigner-Seitz volumes of atoms. For

transition-metal vacancies, we used Fermi energies from band-structure calculations by Sigalas, Papaconstantopoulos and Bacalis [4]. For the Al vacancy, the Fermi energy was calculated in the free electron approximation assuming 3 conduction electrons per atom.

*Table I.* Work functions and atomic volumes.

Element	Work functions $\phi$ (eV) (from ref. [3])	Optimized work functions $\phi$ (eV)	Atomic volume $\Omega$ (nm <sup>3</sup> )
V	4.25	-	0.01385
Nb	4.05	-	0.01798
Ta	4.05	-	0.01799
Cr	4.65	-	0.01200
Mo	4.65	-	0.01558
W	4.80	-	0.01586
Fe	4.93	-	0.01177
Co	5.10	-	0.01099
Rh	5.40	5.75	0.01375
Ir	5.55	-	0.01414
Ni	5.20	-	0.01094
Pd	5.45	5.30	0.01472
Pt	5.65	5.80	0.01511
Cu	4.45	4.55	0.01181
Ag	4.35	4.45	0.01705
Au	5.15	5.02	0.01696
Zn	4.10	-	0.01522
Cd	4.05	-	0.02160
Al	4.20	-	0.01660
Ga	4.10	-	0.01960
In	3.90	-	0.02608
Si	4.70	-	0.02000
Ge	4.55	-	0.02262
Sn	4.15	-	0.02697

### 3. Measurements in cubic metals and intermetallics

The charge transfer model is now applied to interpret quadrupole interactions and binding energies measured for solute atoms or vacancies next to  $^{111}\text{In}/\text{Cd}$  PAC probe atoms. Quadrupole interactions are detected by PAC through the time and angular correlation of successive gamma rays emitted following decay of  $^{111}\text{In}$  to  $^{111}\text{Cd}$ . For further details, the experimental papers cited below should be consulted as well reviews of PAC studies of point defects [5,6,7,8]. While quadrupole interactions are measured using the 247 keV level of the daughter  $^{111}\text{Cd}$  nucleus following electron capture decay of  $^{111}\text{In}$ , binding energies are measured between defects and the parent In atom because jumping rates of atoms in the experiments were too low to allow for a redistribution of defects and solutes between the times of creation and decay of the PAC level.

Solutes. Krzysztof Królás made extensive studies of quadrupole and binding interactions of solutes in noble metals using the PAC probes  $^{111}\text{In}/\text{Cd}$  and  $^{100}\text{Pd}/\text{Rh}$ . His measurements for  $^{111}\text{In}/\text{Cd}$  [9,10,11,12] are tabulated in Table II together with additional results from other researchers [13,14,15]. Third and fourth columns give reported experimental quadrupole interaction frequencies and binding energies (positive signs indicate attractive interactions). Averages are listed where more than one value was available. Reported uncertainties in quadrupole frequencies and binding energies are typically  $\pm 1$  Mrad/s and  $\pm 0.02$  eV. All measured efg asymmetry parameters were consistent with zero, as would be expected if lattice relaxations around the probe atom were isotropic.

To determine binding energies, Królás made series of measurements at elevated temperature: for a given fractional concentration of solute  $c$ , the ratio of site fractions of probes having 1 and 0 defect neighbors in thermal equilibrium is given to a good approximation by

$$f_1 / f_0 = zc \exp(+E_B / k_B T), \quad (4)$$

in which  $z$  is the number of possible defect sites in the first neighbor shell (the coordination number). The binding energies were determined from slopes of Arrhenius plots of the ratios of site fractions.

Column 6 of Table II gives predicted values for the quadrupole interaction up to an arbitrary constant. The sign of the predicted efg is also indicated in Column 6 even though it cannot be determined from a gamma-gamma PAC measurement. Positive signs in column 6 indicate that the solutes have negative defect charges in their hosts; only Zn and Ga in silver and Ag in gold have negative signs. Column 7 gives predicted values for the binding energies of solutes to the parent In probe, up to an arbitrary constant. Positive values indicate that an attractive interaction exists for most systems, again excepting Zn and Ga in silver and Ag in gold. As can be seen from Table I, In has the smallest work function, so its charge in all listed hosts should be positive. The predicted repulsion of Zn, Ga and Ag solutes from In occurs because charges of those solutes are also positive. Notably, there is complete agreement between signs of measured and predicted binding energies. A detailed comparison between experimental and predicted values will be given below.

Table II. Quadrupole interactions and binding energies of solutes with  $^{111}\text{In}/\text{Cd}$  probes in noble metal hosts.

Host	Solute	$\omega_0$ (Mrad/s)	$E_B$ (eV)	Measurement references	Quadrup. int. par.	Binding energy par.
					$-\Delta\phi_{HS}/\Omega_H$ (eV/nm <sup>3</sup> )	$-\Delta\phi_{HP}\Delta\phi_{HS}/\Omega_H^{1/3}$ (eV <sup>2</sup> /nm)
Cu	Pd	47.8	0.090	[9, 13]	85	2.42
	Pt	75.0	0.062	[9, 13, 11]	102	2.90
	Rh	75.6	0.086	[13]	90	2.29
Ag	Pd	41.2	0.133	[10, 13]	65	1.92
	Pt	72.0	0.171	[10, 13]	76	2.27
	Cu	5.0	0.012	[10, 12]	6	0.17
	Zn	15.1	-0.069	[10, 12]	-15	-0.44
	Ga	13.2	-0.113	[10, 12]	-15	-0.44
	Au	25.0	0.025	[10, 12, 14, 15]	47	1.40
	Rh	70.8		[13]	62	1.84
Au	Pd	13.2	0.130	[10, 13]	18	1.46
	Pt	36.6	0.122	[10, 13]	29	2.43
	Ag	21.5	-0.025	[14, 10]	-47	-3.89
	Rh	33.6		[13]	15	1.22

**Vacancies.** Quadrupole interactions and binding energies of vacancies next to In probe atoms have been measured in *fcc* metals (ref. [7] and references therein), *bcc* metals [16,17,18,19] and CsCl phases [20,8,21,22,23,24]. We restrict ourselves to consideration of complexes of an  $^{111}\text{In}/\text{Cd}$  probe on one lattice site with a single vacancy in the near-neighbor shell. Table III lists measured interactions for vacancies in *fcc* and *bcc* metals and CsCl phases, with typical uncertainties estimated to be  $\pm 1$  Mrad/s and  $\pm 0.025$  eV, and calculated quadrupole and binding interactions. Measured efg asymmetry parameters for all vacancy signals were consistent with zero except for the In-vacancy complex in Al, for which the measured value  $\eta=0.41$  is taken to suggest that an asymmetric atomic relaxation occurred around the probe atom.

For the *fcc* and *bcc* metals, binding energies were determined from measurements of annealing of excess concentrations of vacancies created at low temperature by irradiation. In the course of an isochronal annealing sequence, the onset of vacancy motion leads, in the case of an attractive interaction, to trapping at one temperature and detrapping at a higher temperature. As shown by Pleiter and Hohenemser [7], the trapping temperature  $T_{\text{trap}}$  depends on the vacancy migration energy and initial concentration of excess defects, and the detrapping temperature  $T_{\text{detrapp}}$  depends on the sum of migration and binding energies. Following ref. [7], the binding energy of a vacancy to a probe in an *fcc* metal is given by

$$E_B = k_B T_{\text{detrapp}} \ln(7\nu' t) - k_B T_{\text{trap}} \ln(84\nu_{1V}(0)t / f_{\text{max}}), \quad (5)$$

in which  $t$  is the isochronal annealing time,  $\nu$  and  $\nu'$  are jump attempt frequencies of a vacancy in the untrapped and trapped states ( $\sim 10^{12}$  Hz),  $c_{IV}(0)$  is the initial fractional concentration of vacancies, and  $f_{\max}$  is the maximum observed site fraction of trapped vacancies. The factors 84 and 7 in eq. 5 are equal to the numbers of independent ways in which a vacancy can trap in the first shell of a probe or detrapp from a probe (the factor 7 replaces an incorrect factor 14 in eq. 23 of ref. [7].) Binding energies were determined by us for five *fcc* metals using eq. 5 and data reported in ref. [7]. Results of experiments for four *bcc* metals, published in the form of vacancy site fractions as a function of isochronal annealing temperature, were used by us to determine binding energies in the same way, after making educated guesses about initial defect concentrations  $c_{IV}(0)$ , with the only difference being that the factor 84 in eq. 5 must be replaced by 56.

For the CsCl phases NiAl, CoAl and FeAl,  $^{111}\text{In}$  probes localize on the Al-sublattice and bind with transition-metal vacancies in the nearest-neighbor shell (for a discussion of this point, see ref. [23]). In NiGa and CoGa,  $^{111}\text{In}$  is assumed similarly to replace Ga [21]. Binding energies were determined in this laboratory by means of equilibrium measurements similar to those carried out for solutes in pure metals by Królas. Measurements were made on samples having compositions rich in the transition metal, for which deviations from the stoichiometric composition are accommodated by structural antisite defects, with vacancies becoming thermally activated at elevated temperature. Unlike in the measurements for solutes, the defect concentration  $c$  of vacancies that enters in eq. 4 is not constant in general because vacancies are thermally activated (see e.g. ref. [25] for a detailed discussion of how the vacancy concentration varies with composition and temperature.) A special feature of these CsCl phases is that the effective formation energy is relatively low ( $\sim 0.5$  eV) compared with the vacancy migration energy. This leads to sluggish annealing of excess defects created, e.g., by quenching from high temperature. Indeed, NiAl, CoAl and FeAl each possess a range of several hundred degrees at intermediate temperature in which vacancies can move over atomic distances during measurement, without appreciable annealing of excess vacancies. As a consequence, the defect concentration  $c$  is effectively constant while populations of trapped and untrapped vacancies are in local equilibrium, so that Królas's method could be used to determine binding energies of In-vacancy complexes in NiAl [26], CoAl [21] and FeAl [23]. (The method was developed independently in this laboratory before becoming aware of Królas's prior work.) Experiments were also made on Ni-poor NiAl, in which transition-metal vacancies are structural defects and were present in large and fixed concentrations of 1-4 at.%, from which the binding energy was determined using eq. 4 [22]. The two separate entries for the In-vacancy binding energy in NiAl, 0.22 and 0.154 eV, come respectively from the measurements on Ni-rich and Ni-poor samples.

Columns 6 and 7 in Table III give predicted values for quadrupole interaction frequencies and binding energies obtained using eqs. 2 and 3 with work-function differences obtained using the Fermi energies given in Column 5. For transition metals, Fermi energies were taken from ref. [4]. For the CsCl phases, Fermi energies of the transition-metal constituents (corresponding to the missing atoms) were used. Since the vacancy must be negatively charged, it will be attracted to positively-charged probes (such as In, which has the smallest work function of elements listed in Table I) and repelled from negatively-charged probes (such as Pd, which has one of the largest work functions in Table I).

Table III. Quadrupole interactions and binding energies of vacancies with  $^{111}\text{In}/\text{Cd}$  probes in *fcc* and *bcc* metals and CsCl intermetallic phases. For CsCl phases, the Fermi energy of the transition metal component was used.

Host	$\omega_0$ (Mrad/s)	$E_B$ (eV)	Meas. Refs.	$E_F$ (eV)	Quadrup. int. par.	Binding energy par.
					$fE_F / \Omega_H$ ( $f = 0.20$ ) (eV/nm <sup>3</sup> )	$\Delta\phi_{HP} fE_F / \Omega_H^{1/3}$ (eV <sup>2</sup> /nm)
Al	60		[7]	11.70	141	0.50
Ag	75	0.18	[7]	6.67	78	0.86
Pd	82		[7]	7.69	104	2.51
Au	86	0.2	[7]	7.25	86	1.74
Pt	97	0.38	[7]	8.79	116	3.44
Cu	109	0.24	[7]	9.03	153	1.63
Ni	120		[7]	9.46	173	3.21
Nb	82	0.31	[17]	10.82	120	0.26
Ta	86	0.39	[16]	10.19	113	0.26
Mo	118	0.42	[18]	11.36	146	1.52
W	134	0.71	[19]	11.47	145	1.75
PdIn	103	0	[20]	7.69	90	0.00
NiAl	128	0.22	[8,21]	9.46	159	0.72
NiAl	128	0.154	[22]	9.46	159	0.72
CoGa	137		[21]	10.52	178	0.51
FeAl	141	0.13	[23]	11.81	194	0.77
CoAl	144	0.19	[21,27]	10.52	182	0.77
NiGa	144		[24]	9.46	161	0.48

#### 4. Results

Predicted and measured quadrupole interaction frequencies are plotted versus each other in Fig. 3.

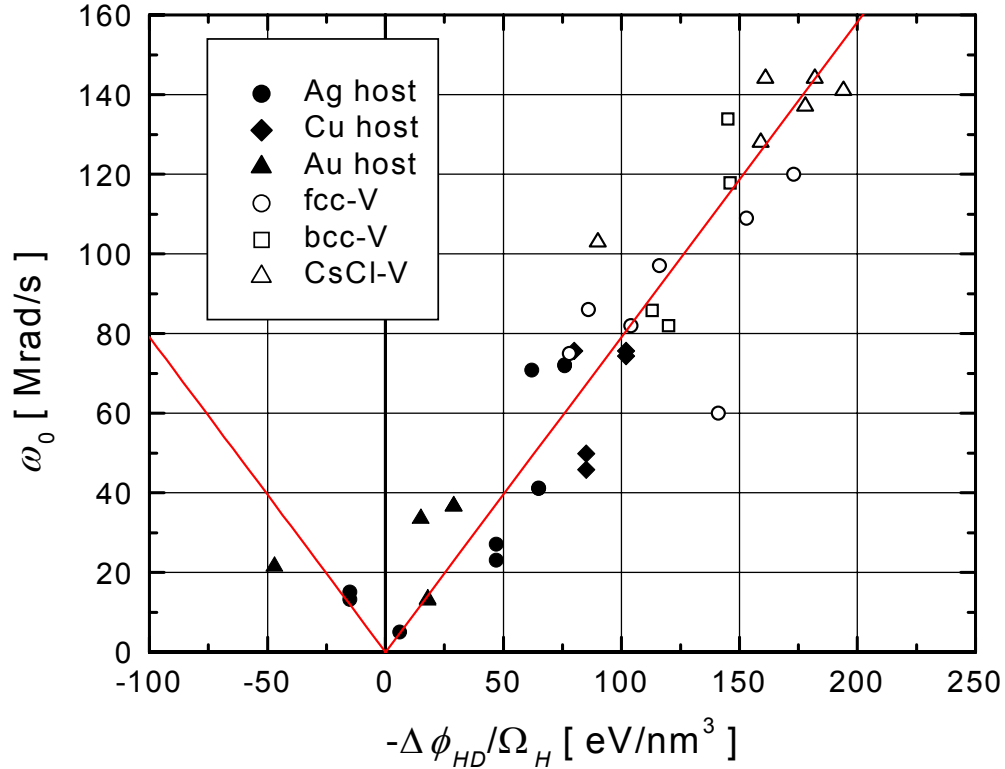


Figure 3. Experimental quadrupole frequencies  $\omega_0$  plotted versus relative frequencies calculated using the charge transfer model with Miedema work functions [3].

Experimental and predicted values are observed to be proportional with each other. Choosing the proportionality factor  $f = 0.20(1)$  made solute and vacancy data sets line up best. The outlying datum with  $\omega_0 = 60$  Mrad/s is for the In-vacancy complex in aluminum, and will be considered separately because it alone has an efg asymmetry parameter significantly different from zero. The drawn line was obtained from a fit of the rest of the data under the assumption that electric field gradients of the three experimental data furthest to the left (at negative abscissas) are opposite in sign to efg's of the rest of the data. The correlation coefficients are  $R = 0.919$  for solute data alone and  $R = 0.883$  for vacancy data alone. Taking together both data sets (less the In-vacancy in Al datum), the correlation coefficient is  $R = 0.962$  and the slope of the fitted, drawn straight line is  $0.79(2)$  (Mrad/s)/(eV/nm<sup>3</sup>).

Local lattice relaxation might also influence quadrupole and binding interactions, for example by altering probe-defect distances or by introducing strain interactions. Various simple approaches were tried to include such effects but were unable to reduce the scatter of data in Fig. 3. Quadrupole interaction strengths also showed no obvious dependence on the row of host or solute atom in the periodic table.

A significant reduction in scatter of the quadrupole interaction data for solutes was obtained by minor adjustments of the Miedema work functions. Charge transfers are proportional to differences of work functions that are small, and are therefore quite sensitive to values assumed for the work functions. The data set for solutes given in Table II is well suited to examine effects of such adjustments because in several entries an element variously appears as host and solute, so that many predicted values of quadrupole interactions are coupled. By trial and error, an optimized set of work functions was found that greatly reduced the scatter of the data, as shown in Figure 4. The optimized work functions are listed in Table I where they differ from those of ref. [3]. Fig. 4 exhibits a correlation coefficient  $R= 0.987$  for the solute data alone and  $R= 0.979$  for all but the Al datum.

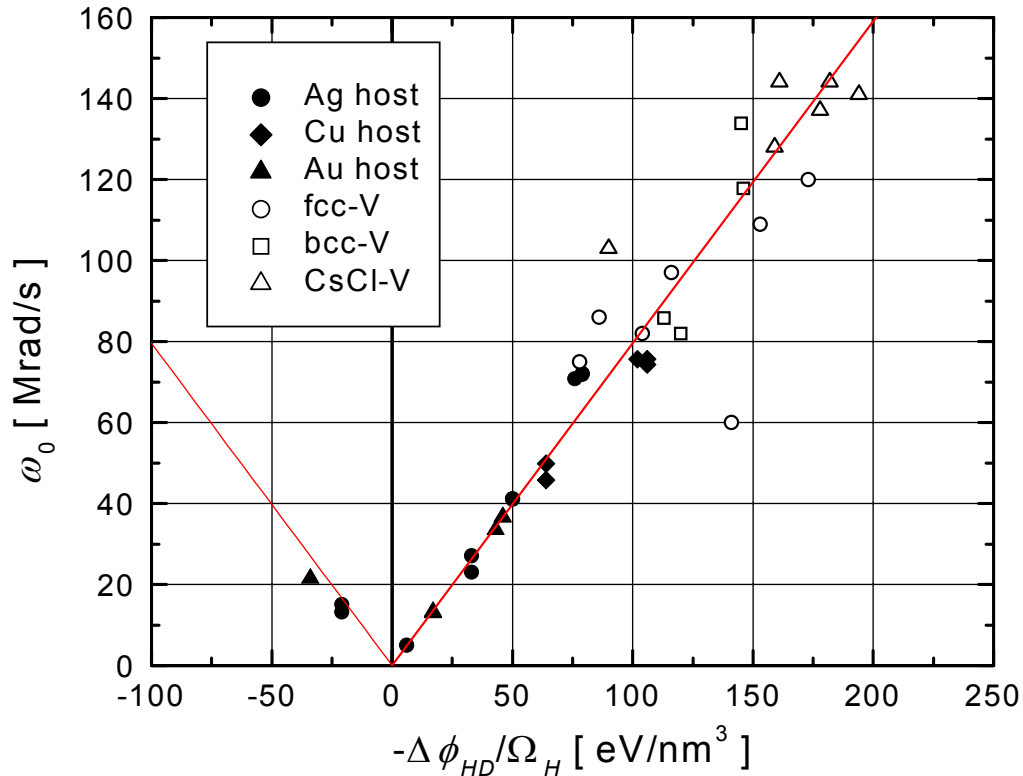


Figure 4. Experimental quadrupole frequencies  $\omega_0$  plotted versus quadrupole interaction parameters calculated using the charge transfer model with optimized work functions listed in Table I.

No attempt was made to optimize predictions of interactions for vacancy complexes since the data are not coupled in the same way as the solute data. Overall, agreement between experimental and predicted values shown in Fig. 4 is good. Accepting the linear correlation shown in Fig. 4, one can examine the consistency of other measurements found in the literature; for example, quadrupole frequencies reported in ref. [28] for  $^{111}\text{Cd}$  probes in silver identified as being next to Cu, Ir, Zn, In and Sn solutes are much greater than expected on the basis of data shown in Fig. 3 or 4. This leads one to question the attributions of frequencies to defect configurations made by the authors.

In Figure 5 are plotted experimental versus predicted binding energies, using the Miedema work functions. A similar plot using the optimized work functions or after adjusting the work function of the In probe did not reduce the scatter significantly.

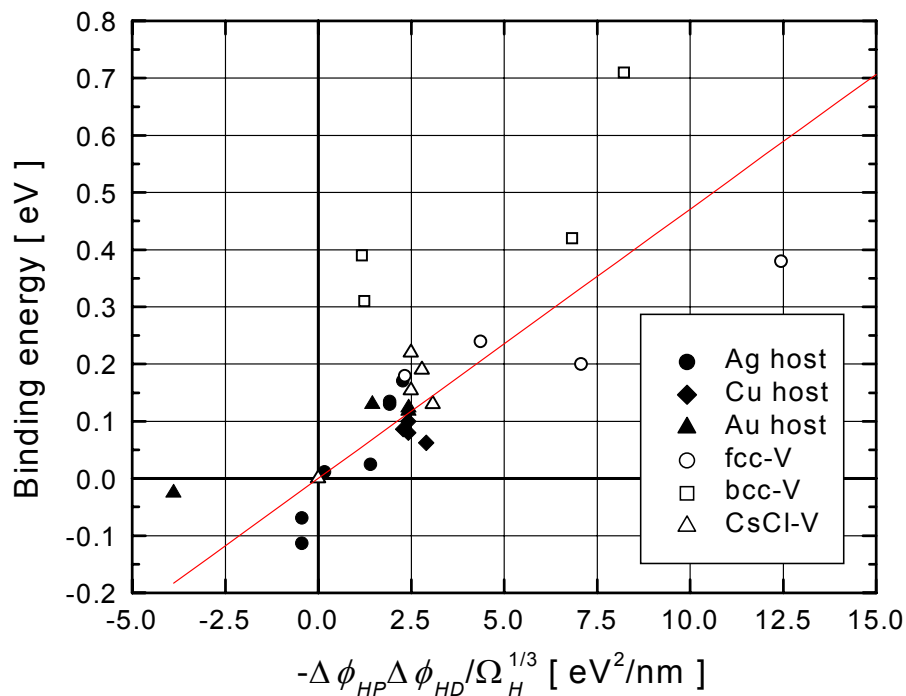


Figure 5. Experimental versus predicted binding energies calculated using Miedema work functions [3].

As can be seen, the correlation coefficient for the data in Fig. 5 is much poorer than for quadrupole interactions, although all data correctly fall in the upper right and lower left quadrants, as they should for attractive and repulsive interactions, respectively. The reason for the poorer correlation is unclear. It might reflect a greater sensitivity of binding energies to strain interactions between probe and defect than quadrupole interactions exhibit. In addition, the relatively large experimental values of binding energies for vacancies in *bcc* metals suggest that crystal structure may have an influence.

## 5. Discussion

Królas parameterized effects of solute and probe charges through nominal valence differences (e.g., in Cu, Ag or Au, In and Pd solutes were assigned charge differences  $\Delta Z$  equal to +2 and -1, respectively [9]). The present parameterization provides for a more subtle treatment of electrostatic interactions, permitting analysis of interactions even for a solute that is nominally isovalent with a host, such as for Ag in Au and *vice versa*.

Quadrupole interactions for  $^{111}\text{Cd}$  are reproduced well, as shown by Fig. 3, and work functions could be optimized to give an excellent correlation for solutes. To test whether the model has more general validity, a significant data set for the  $^{100}\text{Pd/Rh}$  probe measured by Królas (see, e.g., ref. [9]) was examined in the same way as the  $^{111}\text{Cd}$  data. A plot like Fig. 3 (not shown) led to a very poor correlation between experimental and predicted values. This is attributed to the fact that In/Cd and Pd/Rh probes are generally oversized and undersized, respectively, in relation to volumes of host atoms in the systems studied. Unlike for  $^{111}\text{Cd}$ ,  $^{100}\text{Rh}$  measurements all yielded quadrupole interactions with efg asymmetry parameters in the range 0.4-0.8 [9]. Such non-zero values were attributed by Królas to anisotropic local atomic relaxations around the undersized Rh probe, as opposed to symmetric relaxations around the larger In probe [9]. Presumably, significant changes in the principal component of the efg accompany asymmetric relaxations, leading to large changes that cannot be accounted for within the present electrostatic model. It is for this reason that the outlying datum for the In-vacancy complex in aluminum was ignored in the analysis of data in Figs. 3 and 4. Thus, it appears that our model may work well for other oversized probes in cubic hosts that exhibit asymmetry parameters close to zero for near-neighbor defects. While some data exist using the Mössbauer probe  $^{119}\text{Sn}$  [29,30], because of the low nuclear spins ( $<2$ ), the asymmetry parameter cannot be measured and one therefore cannot test whether or not relaxations are isotropic. No other large data set of quadrupole interactions with efg asymmetry parameters is known that could be used to test the model. In summary, on the basis of the good correlations in Figs. 3 and 4, the present model appears to have promise for prediction of quadrupole interaction frequencies for other solutes and vacancies next to oversized probes in other hosts, with an expected accuracy of the order of  $\pm 20\%$  once an initial set of data is in hand.

On the other hand, binding energies are not reproduced well, as shown in Fig. 5. Królas estimated absolute values for the binding energies by considering screening of the conduction electrons in the framework of response of a free electron gas to a defect charge. This leads to oscillations in the density of electrons around the defect (Friedel charge density oscillations) [9]. He also used dielectric response theory as an alternative. The major effect of these approaches is to insert factors in expressions for binding energies that are functions of the Fermi energy of the host [9]. Given uncertainties about the factors, it was thought that further elaboration of our model in similar ways would be unproductive. While our model neglects all effects of lattice relaxations, it successfully predicts the sign of the binding energy for all  $^{111}\text{In}$  data.

H	host: Mo																He			
probe: In/Cd																				
<table border="1" style="margin-left: auto; margin-right: auto;"> <tr><td>element</td></tr> <tr><td><math>\phi</math> (eV)</td></tr> <tr><td><math>\omega_0</math> (Mrad/s)</td></tr> <tr><td><math>E_B</math> (eV)</td></tr> </table>																	element	$\phi$ (eV)	$\omega_0$ (Mrad/s)	$E_B$ (eV)
element																				
$\phi$ (eV)																				
$\omega_0$ (Mrad/s)																				
$E_B$ (eV)																				
Li	<b>Be</b>													<b>B</b>	<b>C</b>	N	O	F	Ne	
2.85	<b>5.05</b>													<b>5.30</b>	<b>6.24</b>					
91	<b>20</b>													<b>33</b>	<b>81</b>					
-0.25	<b>0.06</b>													<b>0.09</b>	<b>0.22</b>					
Na	Mg													Al	Si	P	Se	Cl	Ar	
2.70	3.45													4.20	<b>4.70</b>					
99	61													23	<b>3</b>					
-0.28	-0.17													-0.06	<b>0.01</b>					
K	Ca	Sc	Ti	V	Cr	Mn	<b>Fe</b>	<b>Co</b>	<b>Ni</b>	Cu	Zn	Ga	Ge	<b>As</b>	Se	Br	Kr			
2.25	2.55	3.25	3.80	4.25	4.65	4.45	<b>4.93</b>	<b>5.10</b>	<b>5.20</b>	4.45	4.10	4.10	4.55	<b>4.80</b>						
122	107	71	43	20	0	10	<b>14</b>	<b>23</b>	<b>28</b>	10	28	28	5	<b>8</b>						
-0.34	-0.30	-0.20	-0.12	-0.06	0.00	-0.03	<b>0.04</b>	<b>0.06</b>	<b>0.08</b>	-0.03	-0.08	-0.08	-0.01	<b>0.02</b>						
Rb	Sr	Y	Zr	Nb	Mo	<b>Tc</b>	<b>Ru</b>	<b>Rh</b>	<b>Pd</b>	Ag	Cd	In	Sn	Sb	Te	I	Xe			
2.10	2.40	3.20	3.45	4.05	4.65	<b>5.30</b>	<b>5.40</b>	<b>5.40</b>	<b>5.45</b>	4.35	4.05	3.90	4.15	4.40						
129	114	74	61	30	0	<b>33</b>	<b>38</b>	<b>38</b>	<b>41</b>	15	30	38	25	13						
-0.36	-0.32	-0.21	-0.17	-0.08	0.00	<b>0.09</b>	<b>0.11</b>	<b>0.11</b>	<b>0.11</b>	-0.04	-0.08	-0.11	-0.07	-0.04						
Cs	Ba	La	Hf	Ta	<b>W</b>	<b>Re</b>	<b>Os</b>	<b>Ir</b>	<b>Pt</b>	<b>Au</b>	Hg	Tl	Pb	Bi	Po	At	Rn			
1.95	2.32	3.17	3.60	4.05	<b>4.80</b>	<b>5.20</b>	<b>5.40</b>	<b>5.55</b>	<b>5.65</b>	<b>5.15</b>	4.20	3.90	4.10	4.15						
137	118	75	53	30	<b>8</b>	<b>28</b>	<b>38</b>	<b>46</b>	<b>51</b>	<b>25</b>	23	38	28	25						
-0.38	-0.33	-0.21	-0.15	-0.08	<b>0.02</b>	<b>0.08</b>	<b>0.11</b>	<b>0.13</b>	<b>0.14</b>	<b>0.07</b>	-0.06	-0.11	-0.08	-0.07						
Fr	Ra	Ac																		

Figure 6. Predicted values of quadrupole interaction frequencies and binding energies of  $^{111}\text{In}/\text{Cd}$  probes with solutes in molybdenum. Listed for each solute are the work function  $\phi$ , quadrupole interaction frequency  $\omega_0$  and binding energy  $E_B$ .

To see whether the model can be applied to other probes, we consider measurements of binding energies between  $^{119}\text{Sn}$  probes and seven solutes in iron made by Cranshaw. He found attractive binding energies of +0.28 and +0.10 eV for Pd and Ni [29], +0.05 eV for Co [30], weakly repulsive interactions for V and Cr [30] and strongly repulsive interactions for Al, Si, Ga and Ge solutes [30]. Inserting work functions from Table I into eq. 3, the binding energies for the nine solutes are readily calculated to be in the proportions +0.28, +0.15, +0.09, -0.4, -0.15, -0.4, -0.1, -0.5, and -0.2. There is perfect agreement with the signs of Cranshaw's measurements and semiquantitative agreement with magnitudes of the attractive interactions.

The model allows for rapid prediction of interactions across the periodic table. To illustrate, Fig. 6 shows a table of calculated quadrupole interaction frequencies for the PAC level of  $^{111}\text{Cd}$  and binding energies for In impurities next to solutes in the host metal molybdenum. Such a table is readily generated for the  $^{111}\text{In}/\text{Cd}$  probe in any host, or, with relative values, for any combination of probe and host. The calculation assumes that probes and solutes occupy adjacent substitutional sites in a host, which of course may be untrue for grossly oversized or undersized probes and solutes. Attractive or repulsive interactions between solutes and probe atoms enhance or reduce observed site fractions. Solute having attractive interactions are indicated by shading.

In conclusion, quadrupole and binding interactions of solute and vacancy defects have been calculated in the point-charge approximation using a simple model for charge transfer between host metal and defect. Existing data suggests that the model is useful for oversized probe atoms like  $^{111}\text{In}/\text{Cd}$  and  $^{119}\text{Sn}$ . The model may be useful to interpret other phenomena such as impurity diffusion in metals via a vacancy mechanism. There, an attractive or repulsive interaction between impurity and vacancy can help or hinder diffusion.

## References

1. Schwarz K., P. Blaha and Madsen, G. K. H., Computer Physics Communications (2001)
2. F.R. de Boer et al., Cohesion in Metals: Transition Metal Alloys (North-Holland, Amsterdam 1988).
3. H. Bakker, Enthalpies in Alloys: Miedema's Semi-Empirical Model, Trans Tech Publications, Switzerland, 1998.
4. M. Sigalas, D.A. Papaconstantopoulos and N.C. Bacalis, Phys. Rev. B45 (1992), 5777.
5. Günter Schatz and Alois Weidinger, Nuclear Condensed Matter Physics (Wiley, New York 1996)
6. E. Recknagel, G. Schatz and Th. Wichert, in Hyperfine Interactions of Radioactive Nuclei, ed. J. Christiansen (Springer Topics in Current Physics, vol. 31), p. 133.
7. F. Pleiter and C. Hohenemser, Phys. Rev. B25 (1982), 106.
8. Gary S. Collins, Steven L. Shropshire and Jiawen Fan, Hyperfine Interactions 62 (1990), 1.
9. K. Królas, "Experimental studies of screening charge effects for impurities in Cu, Ag and Au", Report 1184/PL, Institute of Nuclear Physics, Krakow (1982).
10. K. Królas, Hyperfine Interactions 60 (1989), 581-597.
11. K. Królas, Phys. Lett. 85A (1981), 107.
12. M. Sternik, K. Królas and B. Lindgren, Hyperfine Interactions 60 (1990), 873.
13. I.J.R. Baumvol et al., Phys. Rev. B22 (1980), 5115.
14. R. Butt, H. Haas and H. Rinneberg, Physics Letters 60A (1977), 323.
15. F.C. Zawislak et al., Phys. Rev. Lett. 38 (1977), 427.
16. R. Sielemann, H. Metzner, E. Hunger and S. Klaumuenzer, Phys. Lett. 117A (1986), 87.
17. R. Sielemann, H. Metzner, R. Butt, S. Klaumuenzer, H. Haas and G. Vogl, Phys. Rev. B25 (1982), 5555.
18. A. Weidinger, R. Wessner, E. Recknagel and Th. Wichert, Nucl. Inst. Meth. 182/183 (1981), 509.
19. G.J. van der Kolk, K. Post, A. van Veen, F. Pleiter and J.Th.M. de Hosson, Radiation Effects 84 (1985), 131.
20. H.G. Mueller and H. Hahn, Phil. Mag. A50 (1984), 71.
21. G.S. Collins, P. Sinha and M. Wei, Hyperfine Interactions C(1) (1996), 380-4.
22. Matthew O. Zacate and Gary S. Collins, Defect and Diffusion Forum 194-199 (2001), 383-88.
23. Gary S. Collins, Luke S.-J. Peng and Matthew O. Zacate, Defect and Diffusion Forum 213-215 (2003), 107-132.
24. G.S. Collins, unpublished.
25. Gary S. Collins and Praveen Sinha, Hyperfine Interactions 130 (2000), 151.
26. Gary S. Collins, Jiawen Fan and Bin Bai, in Structural Intermetallics 1997, ed. M.V. Nathal et al. (The Minerals, Metals & Materials Society, 1997), pp. 43-52.
27. Jiawen Fan, Ph.D. dissertation, Washington State University, 1992 (unpublished).
28. F.C. Zawislak et al., Phys. Rev. Lett. 38 (1977), 427.
29. T.E. Cranshaw, J. Phys. F: Metal Physics 10 (1980), 323-40.
30. T.E. Cranshaw, Journal de Physique, Colloque C2, supplement 3, vol. 40 (1979), C2-167-8.